Journal of Applied Mathematics and Physics, 2025, 13(6), 2045-2062
https://www.scirp.org/journal/jamp
ISSN Online: 2327-4379
ISSN Print: 2327-4352

Comparison of Hyperelastic Models for Analysis of Human and Pig Skins Behavior

Adji Bone[1], Madahan Bien-Aime Liman Kaoye[2], Blaise Bale Baidi[3], Jean-Bosco Samon[2]

[1]Department of Physics, Faculty of Science, University of Ngaoundéré, Ngaoundéré, Cameroon
[2]Department of Mechanical Engineering, National School of Agro-Industrial Sciences (ENSAI), University of Ngaoundéré, Ngaoundéré, Cameroon
[3]Department of Physics, Faculty of Science, University of Maroua, Maroua, Cameroon
Email: adjiadjijunior@gmail.com, limankaoylims@gmail.com, jboscosamon@gmail.com, balebaidi.blaise@yahoo.com

How to cite this paper: Bone, A., Liman Kaoye, M.B.-A., Baidi, B.B. and Samon, J.-B. (2025) Comparison of Hyperelastic Models for Analysis of Human and Pig Skins Behavior. *Journal of Applied Mathematics and Physics*, **13**, 2045-2062.
https://doi.org/10.4236/jamp.2025.136114

Received: April 17, 2025
Accepted: June 17, 2025
Published: June 20, 2025

Abstract

The study of the mechanical behavior of skin tissue is essential for various biomedical applications, ranging from reconstructive surgery to the design of medical devices. This work compares hyperelastic energy models to characterize the mechanical behavior of human and porcine skin tissue. The analysis is based on experimental data by Gunner *et al.* and Lim *et al.*, obtained from uniaxial extension tests of human and porcine skin respectively. The Beda-Chevalier step-by-step approach is combined with non-linear least squares to identify the rheological parameters of five hyperelastic energy models: Mooney-Rivlin, Yeoh, Ogden, Fung and Veronda-Westmann. The comparison between theoretical results and experimental data shows that, apart from the partial Mooney-Rivlin model, the other models offer good accuracy in representing the non-linearity of skin tissue. In particular, the Yeoh, Ogden and Veronda-Westmann models have the smallest mean errors, with values ranging from 0.029% to 0.127% for all the experimental data considered in this work. The results and conclusions provided demonstrate the importance of this study and its contribution to the choice of a hyperelastic model for skin tissue modelling, which has direct implications for biomechanics and clinical applications.

Keywords

Hyperelastic Models, Uniaxial Extension, Beda-Chevalier Method, Human and Porcine Skin Tissue

1. Introduction

The skin covers almost the entire body and is the largest organ after the skeleton and muscles. Being very supple, the skin allows unequalled freedom of movement

and the ability to grip objects, permits a multitude of exchanges with the outside world, forms a physical barrier that protects the organs against external aggression (mechanical, chemical, microbial, sunlight, etc.), regulates temperature and performs various hormonal functions. From an architectural point of view, the skin, whether human or animal, is a complex biological structure essentially made up of three layers: the epidermis, the dermis and the hypodermis [1]. This structural complexity gives the skin diverse mechanical properties, described in the literature as: hyperelasticity, non-linearity [1]-[5], viscoelasticity [6] [7], anisotropy [8]-[10] and pre-tension in the natural state [11] [12].

Knowledge of the mechanical behavior of the skin has long attracted the interest of several research specialties such as dermatology, cosmetology, surgery and biomechanics, particularly for digital modelling in surgery, the design of prostheses and tissue engineering. Plastic and reconstructive surgery, in particular, is the field most concerned with the mechanical properties of the skin, where the optimization of surgical procedures is becoming increasingly stringent. When the skin is damaged in an accident, for example, skin continuity has to be reconstituted. This becomes particularly difficult when a significant amount of skin has been lost, as the surrounding skin must be extended to cover the wound [13]. In such circumstances, the mechanical properties of the skin are a key feature, in determining its level of extensibility. Wound closure will be much easier with soft, elastic skin than with rigid, inextensible skin [14]. More often than not, the skin is assessed by the clinician using his or her senses, in particular touch and sight, which do not provide precise information on the mechanical behavior of the skin and more often than not lead to heterogeneous results. The development of devices and methods for objectively assessing the mechanical properties of the skin would make diagnosis more rational, safer and therefore more beneficial.

Various mechanical techniques and procedures have been used to study the mechanical properties of skin, including: tensile tests (uniaxial or multiaxial) [15]-[17], extensometry tests [18]-[21], torsion tests [22] [23], indentation tests [24]-[26] and suction tests [27]-[29]. These various experimental techniques have enabled us to acquire considerable knowledge about the mechanical properties of the skin, but the results obtained need to be validated by rigorous mathematical modelling involving hyperelastic energy models [30] [31]. Nevertheless, despite the progress made in modelling the mechanical behavior of skin tissue and the abundance of existing hyperelastic models, there are still uncertainties regarding the choice of the most appropriate model to represent the mechanical behavior of skin tissue. Indeed, while there are a variety of models used to characterize the skin, there is no standard model for modelling skin tissue.

The aim of this work is to compare several commonly used hyperelastic models (Mooney-Rivlin, Yeoh, Ogden, Fung and Veronda-Westmann) to characterize the behavior of human and pig skin. The Beda-Chevalier stepwise approach is combined with non-linear least squares to obtain the analytical responses of the different models. The results obtained with each model are compared with experi-

mental data from extension tests, in order to assess the suitability of the models for describing the mechanical behavior of skin tissue, identify the model offering the best fit to the experimental data and propose recommendations for biomechanical applications.

2. Continuum Mechanics Theory and Constitutive Equations in Large Deformations

In this section, we review a number of concepts in continuum mechanics that lead to the formulation of behavior laws in large deformations.

Let us consider the deformation of a soft solid and denote $\boldsymbol{F}$ the deformation gradient tensor. The behavior law of these types of solids, described as hyperelastic, is generally derived from a hyperelastic energy potential W. For isotropic materials (e.g., rubbers), the deformation energy function can be represented in terms of the invariants (I_1, I_2, I_3) of the right Cauchy-Green tensor $\boldsymbol{C}$ or the eigenvalues of the deformation gradient tensor $\boldsymbol{F}$, called principal extensions $(\lambda_1, \lambda_2, \lambda_3)$.

$$W = (I_1, I_2, I_3) = W(\lambda_1, \lambda_2, \lambda_3) \tag{1}$$

The deformation gradient tensor $\boldsymbol{F}$ is given by:

$$\boldsymbol{F} = \frac{\partial \boldsymbol{x}}{\partial \boldsymbol{X}} = Grad\boldsymbol{x} \tag{2}$$

The right Cauchy-Green tensor $\boldsymbol{C}$ is obtained from $\boldsymbol{F}$ by the relation:

$$\boldsymbol{C} = \boldsymbol{F}^t \boldsymbol{F} \tag{3}$$

And the left Cauchy-Green tensor $\boldsymbol{B}$:

$$\boldsymbol{B} = \boldsymbol{F}\boldsymbol{F}^t \tag{4}$$

The invariants (I_1, I_2, I_3) associated with $\boldsymbol{C}$ are given by:

$$\begin{cases} I_1 = tr(\boldsymbol{C}) \\ I_2 = (tr(\boldsymbol{C}))^2 - tr(\boldsymbol{C}^2) \\ I_3 = \det \boldsymbol{C} \end{cases} \tag{5}$$

To establish the behavior laws, we consider a unit cube deforming into a parallelepiped of dimensions λ_1, λ_2 et λ_3, keeping its sides parallel to the sides of the undeformed cube shown in Figure 1 below [32].

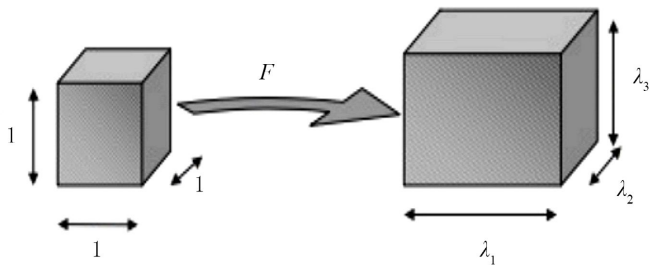

Figure 1. Deformation of an elementary cube into a parallelepiped.

The deformation gradient tensor $\boldsymbol{F}$ for the corresponding transformation is written as:

$$\boldsymbol{F} = \begin{bmatrix} \lambda_1 & 0 & 0 \\ 0 & \lambda_2 & 0 \\ 0 & 0 & \lambda_3 \end{bmatrix} \tag{6}$$

By introducing the expression for the deformation gradient tensor $\boldsymbol{F}$ given in Equations (6) into (3) and (4), we obtain the right and left Cauchy-Green tensors $\boldsymbol{C}$ and $\boldsymbol{B}$ respectively as:

$$\boldsymbol{C} = \boldsymbol{F}^t \boldsymbol{F} = \begin{bmatrix} \lambda_1^2 & 0 & 0 \\ 0 & \lambda_2^2 & 0 \\ 0 & 0 & \lambda_3^2 \end{bmatrix} \tag{7}$$

And

$$\boldsymbol{B} = \boldsymbol{F}\boldsymbol{F}^t = \begin{bmatrix} \lambda_1^2 & 0 & 0 \\ 0 & \lambda_2^2 & 0 \\ 0 & 0 & \lambda_3^2 \end{bmatrix} \tag{8}$$

From (7) we derive the invariants I_1, I_2 and I_3 of $\boldsymbol{C}$:

$$\begin{cases} I_1 = tr(\boldsymbol{C}) = \lambda_1^2 + \lambda_2^2 + \lambda_3^2 \\ I_2 = \left(tr(\boldsymbol{C})\right)^2 - tr\left(\boldsymbol{C}^2\right) = \lambda_1^2\lambda_2^2 + \lambda_1^2\lambda_3^2 + \lambda_2^2\lambda_3^2 \\ I_3 = \det \boldsymbol{C} = \lambda_1^2\lambda_2^2\lambda_3^2 \end{cases} \tag{9}$$

In uniaxial extension, the specimen is stretched along one of the directions of the axes, the other free facets of the specimen are not subjected to external forces and are in a state of zero stress.

Considering the reference frame linked to the specimen and following the direction of extension, the main elongations for the case of uniaxial extension can be written as:

$$\lambda_1 = \lambda, \ \ \lambda_2 = \lambda_3 = \frac{1}{\sqrt{\lambda}} \tag{10}$$

The first two invariants of the deformation gradient tensor can be written as Equation (11) below:

$$\begin{cases} I_1 = \lambda^2 + \dfrac{2}{\lambda} \\ I_2 = 2\lambda + \dfrac{1}{\lambda^2} \end{cases} \tag{11}$$

By replacing the main extensions given in Equation (10) in the formulation (6), we obtain the expression of the deformation gradient tensor for the uniaxial deformation mode:

$$\boldsymbol{F} = \begin{bmatrix} \lambda & 0 & 0 \\ 0 & \dfrac{1}{\sqrt{\lambda}} & 0 \\ 0 & 0 & \dfrac{1}{\sqrt{\lambda}} \end{bmatrix} \tag{12}$$

The left Cauchy-Green tensor $\boldsymbol{B}$ is deduced from the deformation gradient tensor in Equation (12):

$$\boldsymbol{B} = \boldsymbol{F}\boldsymbol{F}^{\mathrm{T}} = \begin{bmatrix} \lambda^2 & 0 & 0 \\ 0 & \dfrac{1}{\lambda} & 0 \\ 0 & 0 & \dfrac{1}{\lambda} \end{bmatrix} \Rightarrow \quad \boldsymbol{B}^2 = \begin{bmatrix} \lambda^4 & 0 & 0 \\ 0 & \dfrac{1}{\lambda^2} & 0 \\ 0 & 0 & \dfrac{1}{\lambda^2} \end{bmatrix} \tag{13}$$

In the Eulerian formulation, the expression for the stress is given by:

$$\boldsymbol{\sigma} = \left[\left(\frac{\partial W}{\partial I_1} + I_1 \frac{\partial W}{\partial I_2} \right) \boldsymbol{B} - \frac{\partial W}{\partial I_2} \boldsymbol{B}^2 \right] - p\boldsymbol{I} \tag{14}$$

By replacing $\boldsymbol{B}$ and $\boldsymbol{B}^2$ in Equation (13) and the invariants in Equation (11) in Equation (14), we obtain the components of the Cauchy stress tensor in the case of uniaxial extension:

$$\begin{cases} \sigma_{11} = 2\lambda^2 \dfrac{\partial W}{\partial I_1} + 4\lambda \dfrac{\partial W}{\partial I_2} - p \\ \sigma_{22} = \sigma_{33} = \dfrac{2}{\lambda} \dfrac{\partial W}{\partial I_1} + 2\left(\dfrac{1}{\lambda^2} + \lambda \right) \dfrac{\partial W}{\partial I_2} - p \end{cases} \tag{15}$$

Since the state of stress associated with this mode of deformation is plane, *i.e.* $\sigma_{22} = \sigma_{33} = 0$, we determine the pressure $\boldsymbol{p}$ from the second equation of the system (15):

$$p = \frac{2}{\lambda} \frac{\partial W}{\partial I_1} + 2\left(\frac{1}{\lambda^2} + \lambda \right) \frac{\partial W}{\partial I_2} \tag{16}$$

By replacing $\boldsymbol{p}$ in the first equation of the system (15) we obtain the following behavior law for the case of uniaxial extension:

$$\boldsymbol{\sigma}_{11} = \boldsymbol{\sigma} = 2\left(\lambda^2 - \frac{1}{\lambda} \right) \left(\frac{\partial W}{\partial I_1} + \frac{1}{\lambda} \frac{\partial W}{\partial I_2} \right) \tag{17}$$

The associated nominal stress is:

$$\boldsymbol{\sigma}_n = 2\left(\lambda - \frac{1}{\lambda^2} \right) \left(\frac{\partial W}{\partial I_1} + \frac{1}{\lambda} \frac{\partial W}{\partial I_2} \right) \tag{18}$$

Having laid the theoretical foundations of the mechanics of continuous media in large deformations and presented the general constitutive equations that govern the behavior of materials, we now need to look at the models. These models enable the behavior of materials to be translated into concrete terms, using appropriate mathematical laws, as a function of their nature and the stresses to which they are subjected. They are an essential step in the development of reliable numerical simulations and the interpretation of mechanical phenomena observed in large deformations.

3. Constitutive Hyperelastic Models

Because of the structural complexity of skin tissue and its highly non-linear be-

havior, the continuum mechanics approach, namely the theory of hyperelasticity, involving energy models has been used extensively for its modelling. However, despite a wide variety of deformation energy functions being formulated, the problem of choosing a model that best assesses the behavior of skin tissue remains. Thus, the choice of an energy model is fundamentally guided by a number of criteria, including the number of parameters to be identified, the form of the energy (polynomial, exponential or power, partial or complete, etc.), the extensive use in biomechanical literature and the ability to adapt to the experimental data [33]-[35].

Considering these criteria, the models of Mooney-Rivlin, Yeoh, Ogden, Fung, and Veronda-Westmann have been chosen in this article.

This section presents the different energy models used in this work and the related behavior laws. The different formulations of these models are summarized in Table 1 below.

Table 1. Hyperelastic energy models and their behavior laws.

Model	Strain energy function	Behavior law
Mooney-Rivlin	$W_{MR} = C_{10}(I_1 - 3) + C_{01}(I_2 - 3)$ C_{10} and C_{01}, parameters to be identified	$\sigma = 2\left(\lambda - \frac{1}{\lambda^2}\right)\left(C_{10} + \frac{1}{\lambda}C_{01}\right)$
Yeoh	$W_{Yeoh} = C_{10}(I_1 - 3) + C_{20}(I_1 - 3)^2 + C_{30}(I_1 - 3)^3$ C_{10}, C_{20} and C_{30} are the three parameters	$\sigma = 2\left(\lambda - \frac{1}{\lambda^2}\right)\left(C_{10} + 2C_{20}(I_1 - 3) + 3C_{30}(I_1 - 3)^2\right)$
Ogden	$W_{Og} = \sum_{p=1}^{N} \frac{\mu_p}{\alpha_p}\left(\lambda_1^{\alpha_p} + \lambda_2^{\alpha_p} + \lambda_3^{\alpha_p} - 3\right)$ μ_p and α_p: characteristic parameters	$\sigma = \sum_{p=1}^{N} \mu_p \left(\lambda^{\alpha_p - 1} - \lambda^{-\left(\frac{\alpha_p}{2}+1\right)}\right)$
Fung	$W_{Fu} = \frac{C}{2\beta}\left(e^{\beta(I_1-3)} - 1\right)$ C and β: the model parameters.	$\sigma = C\left(\lambda - \frac{1}{\lambda^2}\right)e^{\beta(I_1-3)}$
Veronda-Westmann	$W_{V-W} = C_1\left(e^{\beta(I_1-3)} - 1\right) - C_2(I_2 - 3)$ C_1, C_2 and β: characteristic properties	$\sigma = 2\left(\lambda - \frac{1}{\lambda^2}\right)\left(C_1\beta e^{\beta(I_1-3)} - \frac{C_2}{\lambda}\right)$

The development and formulation of constitutive models are based on theoretical hypotheses that must be confronted with the physical reality of materials. In order to validate these models or adjust their parameters, it is essential to rely on experimental data. These data not only allow us to characterize the actual behavior of materials, but also to calibrate and assess the relevance of the models. The following section therefore presents the experimental data that will serve as a reference for the analysis of the energy models presented here.

4. Experimental from Human and Porcine Skin

To examine the effectiveness or failure of the different models considered in this work, we choose two sets of experimental data from the literature.

❖ **Gunner *et al*. experimental data**

The first set of data comes from Gunner *et al*. [36], who applied their version of the extensometer to healthy skin in vivo in the human armpit. The tongues of their instrument were 20 mm long and 10 mm wide, and were initially spaced 10 mm apart. They presented time-force and time-extension data that were digitized and converted to nominal stress as a function of extension assuming an initial thickness of 1 mm and an initial width equal to the width of the extensometer tabs (10 mm) [37].

❖ **Lim *et al*. experimental data**

The second set of data is from Lim *et al*. [38] who carried out uniaxial extension tests on the dorsal part of the pig. The specimens were 40 mm long, 25 mm wide and 2 mm thick. They were divided into two groups according to the directions of loading: one group of specimens was cut in the longitudinal direction of the pig's spine. The other group was cut perpendicular to the pig's spine. An MTS 810 testing machine was used to perform the quasi-static tensile experiments. The tensile load and displacement were measured directly by a load cell with a capacity of 220.24 N (50 lbf) and an extensometer of ±1.25 mm, respectively.

The experimental data of Gunner *et al*. [36] and Lim *et al*. [38] from uniaxial extension tests on human and porcine skin were chosen because of the methodological quality of their experimental protocols and their recognized relevance for the comparative study of the mechanical properties of skin tissues. The use of uniaxial extension data to characterize skin tissue is explained by the experimental simplicity of this type of test, its ability to provide precise information on mechanical behavior in a given direction, and its relevance as a first approximation of the mechanical properties of soft tissues. In addition, uniaxial extension provides stress-strain curves that can be used to efficiently adjust constitutive models, while being more reproducible and less expensive than other stress modes such as biaxial or shear tests. However, the future integration of data from biaxial tensile or shear tests is essential to rigorously assess the validity of the models, particularly in areas where the real stresses are complex.

The experimental data presented constitute an essential basis for identifying the rheological parameters of the materials studied. The behavior laws formulated from the models must be fed with parameters that reflect the actual mechanical properties of the material. The next step is, therefore, to use the experimental data to identify the characteristic parameters of the material, using appropriate adjustment and optimization techniques.

5. Identification of Rheological Parameters

Identifying the rheological parameters of a hyperelastic model is an essential step in describing the behavior of a hyperelastic material. It consists of matching a theoretical solution σ_{the} resulting from a hyperelastic energy model with the experimental data represented by the pair of points (λ_{exp} , σ_{exp}).

In the literature, several methods have been adopted to identify the parameters

of a hyperelastic energy model. These include the least squares method [39]-[41], the Levenberg-Marquard method [34] [42], the Beda-Chevalier method [39] [43] [44], the genetic algorithm method [45] [46], the particle swarm optimisation algorithm [47], etc… In this work, we use the Beda-chevalier method coupled with the method of least squares to identify the rheological parameters of the various models selected. The challenge of combining these two methods lies in the fact that each individual method has limitations or approximations that can lead to less accurate results. By combining these two methods, we can take advantage of their respective benefits and reduce the errors inherent in each method.

The identification process is, therefore, based on a two-stage methodological approach:

1) The parameters are first identified using the Beda-Chevalier method and introduced into the behavior law of the corresponding model:

- If the results obtained are satisfactory, the parameters are retained;
- if the results are unsatisfactory, the parameters obtained are considered as initial values for the least squares method;

2) We apply the least squares method to refine the results obtained by the Beda-Chevalier method.

These identification stages are summarized in the flow chart below.

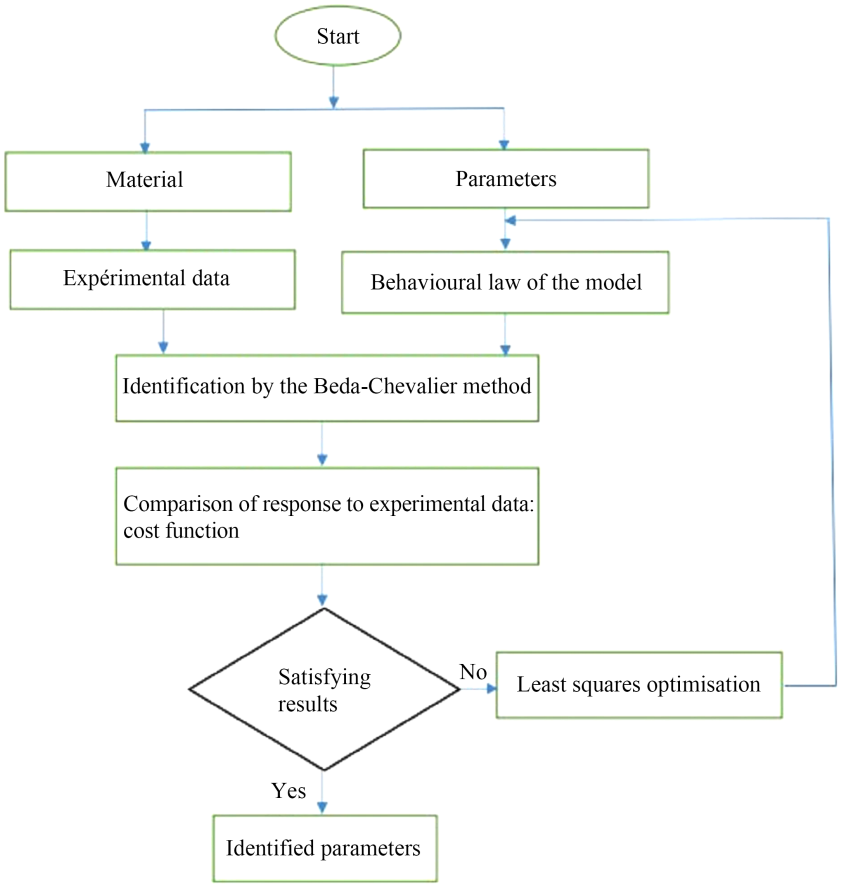

Figure 2. Principle for identifying rheological parameters.

Once the rheological parameters have been identified from the experimental data, the constitutive models can be used to simulate the behavior of the material and assess their predictive capacity. The following section is devoted to the presentation and analysis of the results obtained. These results make it possible to assess the relevance of the models used, to measure any discrepancies and to consider avenues for improvement.

6. Results

This section deals with the presentation and analysis of the results obtained. The results presented here are those obtained on the experimental data of Gunner *et al.* (human skin) and the data of Lim *et al.* (pig skin) in simple extension. Table 2 reconciles the values of the parameters of the different models identified by the Beda-Chevalier method combined with least squares.

Table 2. Values of the rheological parameters of the various hyperelastic models obtained from human and pig skin data.

Models	Parameters	Gunner *et al.* data	Lim *et al.* data (Perpendicular to spine)	Lim *et al.* data (Parallel to spine)	Unit
Mooney-Rivlin	C_{10}	330.2	18.34	26.7	kPa
	C_{01}	9.124×10^{-6}	1.828×10^{-7}	2.271×10^{-8}	kPa
Yeoh	C_{10}	91.69	2.000	8.462	kPa
	C_{20}	917	3.062	16.76	kPa
	C_{30}	1.484×10^{-5}	0.2057	0.9145	kPa
Ogden	α	12.92	6.014	7.32	/
	μ	33.33	1.788	4.722	kPa
Fung	C	300	12.07	24.6	kPa
	β	5.797	0.4798	1.413	/
Veronda-Westmann	C_1	737.7	43.92	38.93	kPa
	C_2	859.5	14.39	22.33	kPa
	β	1.201	0.2987	0.7321	/

The ability of the different models whose behavior laws are defined in section 3 to predict the behavior of human and porcine skin tissues is evaluated in this part of the work. By replacing the different values of the rheological parameters summarized in the table above in these behavior laws, we obtain the stress-strain curves of the different models, in comparison with the experimental data, represented in Figures 3-5.

The results presented provide qualitative information on the behavior of human and porcine skin tissue. It is now necessary to analyze these results, in order

to discuss the consistency between the theoretical responses and the experimental data. The following section provides a critical discussion of the results, highlighting the strong points, the discrepancies observed and the implications for modelling skin tissue under large deformations.

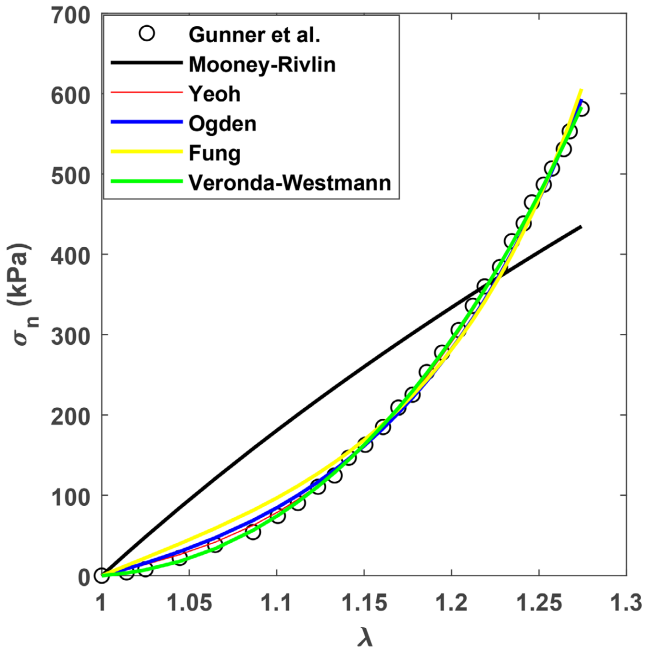

Figure 3. Hyperelastic models prediction compared to human skin data from Gunner *et al.* [46].

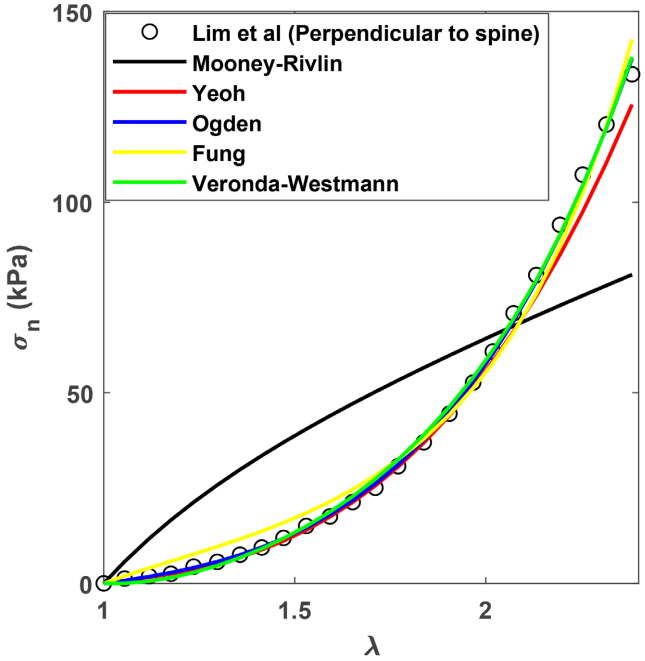

Figure 4. Hyperelastic models prediction compared to pig skin data (perpendicular to spine) from Lim *et al.*

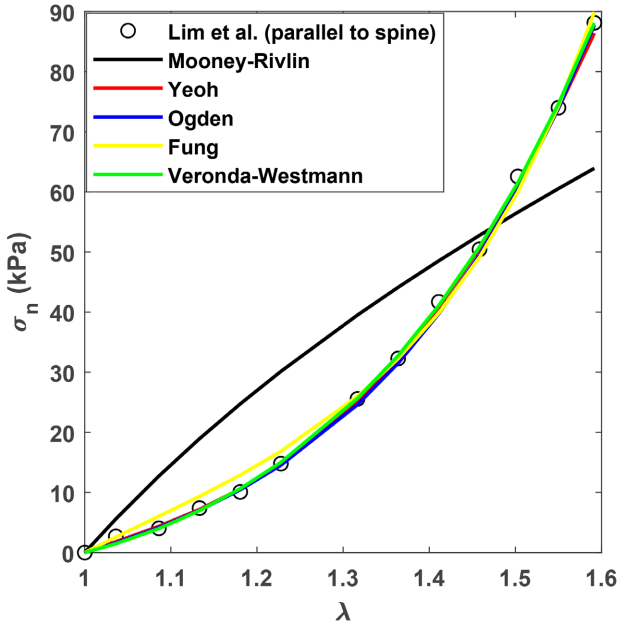

Figure 5. Hyperelastic models prediction compared to pig skin data (parallel to spine) from Lim *et al.*

7. Discussion

The results obtained are processed by analyzing the various relative errors between the experimental data and the theoretical responses of the five hyperelastic models used in this work. This analysis consists of highlighting the model with the minimum deviation from the data, in order to identify the most suitable model for each skin tissue. We calculate the relative error on the basis of the relationship below:

$$Error = \frac{\left|\sigma_{\text{exp}} - \sigma_{\text{the}}\right|}{\sigma_{\text{exp}}} \tag{19}$$

where σ_{exp} represents the experimental data and σ_{the} the theoretical response of the model.

Figures 6-8 show the error curves illustrating the differences between the analytical responses and the experimental skin tissue data.

Examination of Figures 3-5 shows that both types of tissue (human and porcine) exhibit the non-linear behavior typical of biological materials, represented by a J-shape. Human skin exhibits greater tensile stiffness, while porcine skin tissue shows greater deformability. This observation can be interpreted by the fact that in human skin, collagen fibers, which are stiffer than elastin fibers, are directly stressed. Thus, because of their high rigidity, collagen fibers deform very little under high stress, allowing human skin to deform less than pig skin. It should also be noted that collagen fibers have a non-negligible influence on the overall stiffness of the material in large deformation, which is closely linked to the parameters of the models. This justifies the disparity in the parameters obtained for the two tissues, summarized in Table 2.

Concerning the fit of the hyperelastic models, Figure 6 shows that with the data from Gunner *et al.* [36], the relative errors are of the order of 0% to 6%:

- 0% to 6% for the Mooney-Rivlin model;
- 0% to 2.2% for the Fung model;
- 0% to 1.2% for the Ogden model;
- 0% to 1% for the Yeoh model;
- 0% to 0.3% for the Veronda-Westmann model.

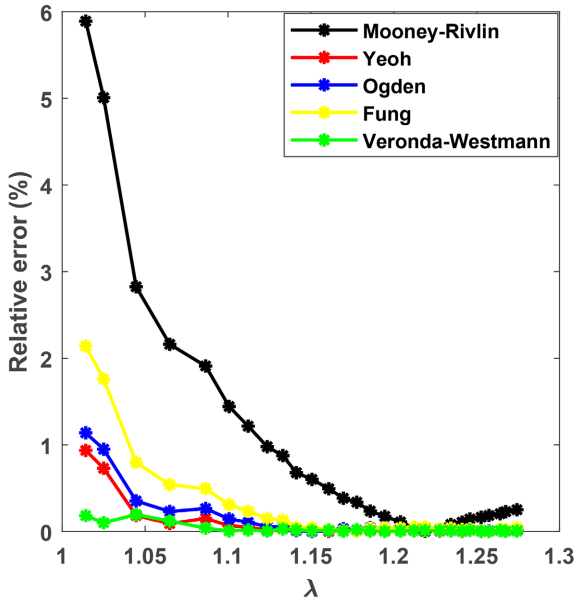

Figure 6. Relative error between the experimental data of Gunner *et al.* and the theoretical responses.

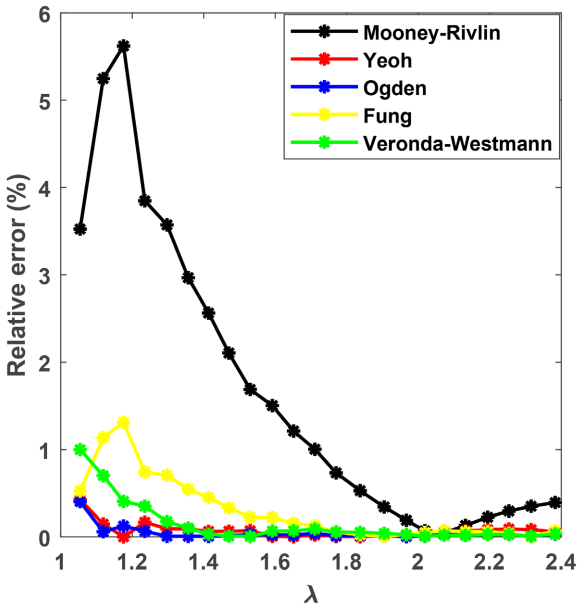

Figure 7. Relative error between the experimental data of Lim *et al.* (perpendicular to the spine) and the theoretical responses.

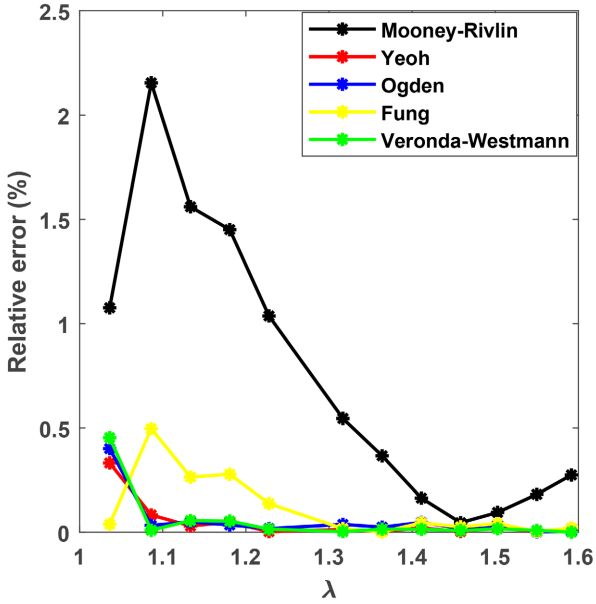

Figure 8. Relative error between the experimental data of Lim *et al.* (parallel to the spine) and the theoretical responses.

The values presented in **Table 2** allow the last four models to correlate better with the data, as the errors determined for these models are insignificant. Analysis of the different errors confirms the results in **Figure 3**, which show that these four models correlate well with the experimental data. Furthermore, the inability of the Mooney-Rivlin model to describe the behavior of this material is due, on the one hand, to its partial nature and, on the other hand, to the linear aspect of the behavioral law of this energy model. These results corroborate those obtained by Martins *et al.* [34] on rubbers and biological tissues.

Figure 7 and **Figure 8** show the relative errors between the Lim *et al.* [38] data obtained for loads perpendicular and parallel to the pig's spine and the analytical responses. For the Mooney-Rivlin model, we obtain maximum errors of 5.7% and 2.4% respectively for the directions perpendicular and parallel to the pig's spine. These discrepancies may explain once again the poorer performance of this model (**Figure 4** and **Figure 5**).

We also observe that for the Lim *et al.* [38] data (**Figure 7** and **Figure 8**), the minimum errors are obtained with the Yeoh, Ogden and Veronda-Westmann models. We, therefore, agree with Cora Wex *et al.* [33] and Martins *et al.* [34] that in all biological tissues, models with exponential or polynomial formulae fit the experimental data better. However, the number of parameters has a considerable influence on the performance of a model when fitted to experimental data [33]-[35].

The relative error curves obtained for each of the hyperelastic models studied (Mooney-Rivlin, Yeoh, Ogden, Fung and Veronda-Westmann) made it possible to visually analyze the goodness of fit of these models in relation to the experimental data of Gunner *et al.* [36] and Lim *et al.* [38]. However, visual analysis

alone is not sufficient to quantify precisely the discrepancies between the models and the experimental observations. Therefore, the relative errors were averaged over all the experimental points for each model, making it possible to obtain a comparative table of overall performance and to identify the best-performing models in terms of fit to the experimental data.

Table 3. Summary table of average relative errors.

Model	Error (%) compared with data from Gunner *et al.* (human skin)	Error (%) with respect to Lim *et al.* data (perpendicular to the pig's spine)	Error (%) with respect to Lim *et al.* data (parallel to the pig's spine)
Mooney-Rivlin	0.954	1.660	0.746
Yeoh	0.0882	0.074	0.051
Ogden	0.123	0.042	0.0834
Fung	0.240	0.300	0.127
Veronda-Westmann	0.02901	0.143	0.067

Analysis of the values summarized in Table 3 shows that the Yeoh, Ogden and Veronda-Westmann models have the best overall performance, with the lowest relative errors in the two tissue cases. This consistency in results suggests that these models are suitable for accurate modelling of the hyperelastic behavior of the tissues under consideration.

8. Conclusion

The aim of the research presented in this manuscript is to compare and describe the ability of models to characterize the mechanical behavior of human and porcine skin tissue. The identification methods used in this work enabled us to obtain satisfactory results. The analysis and interpretation of the various results show that the polynomial or exponential models, particularly those based on the Fung, Yeoh, Ogden and Veronda-Westmann formulation, offer a very good correlation for all the experimental data. In particular, the last three models performed remarkably well for all three experimental data sets, with the smallest errors. On the other hand, the Mooney-Rivlin model performed less well due to its simple formulation, which limits its applicability to the entire deformation domain of human and pig skin tissue. Furthermore, although pig skin is frequently used as a substitute model for human skin, significant differences were observed in the estimated mechanical parameters, thus influencing the choice of the most suitable model for each skin tissue. The various results presented in this work could further refine our understanding and prediction of the behavior of skin tissue, and help us to choose a suitable model for biomedical and clinical applications.

Conflicts of Interest

The authors declare no conflicts of interest regarding the publication of this paper.

References

[1] Joodaki, H. and Panzer, M.B. (2018) Skin Mechanical Properties and Modeling: A Review. *Proceedings of the Institution of Mechanical Engineers, Part H: Journal of Engineering in Medicine*, **232**, 323-343. https://doi.org/10.1177/0954411918759801

[2] Shin, H., Han, D., Kim, S. and Rhim, S. (2019) Calibration of Visco-Hyperelastic Model for Tensile Behavior of Porcine Skin. *Archives of Metallurgy and Materials*, **64**, 819-822. https://doi.org/10.24425/amm.2019.129454

[3] Alliliche, W., Renaud, C., Cros, J. and Feng, Z. (2023) Numerical Simulation of Mechanical Tests on a Living Skin Using Anisotropic Hyperelastic Law. *Journal of the Mechanical Behavior of Biomedical Materials*, **141**, Article ID: 105755. https://doi.org/10.1016/j.jmbbm.2023.105755

[4] Alliliche, W., Renaud, C., Cros, J.-M. and Feng, Z.-Q. (2022) Simulation du comportement hyperélastique anisotrope de la peau lors d'un essai d'indentation.

[5] Adam Mohd Adnan, Z., Azman Yahaya, M., Nor Fazli Adull Manan, M. and Mahmud, J. (2018) Quantifying and Comparing the Hyperelastic Properties of Skin, Leather and Silicone. *International Journal of Engineering & Technology*, **7**, 45-49. https://doi.org/10.14419/ijet.v7i4.26.22135

[6] Moučka, R., Sedlačík, M. and Pátíková, Z. (2023) Fractional Viscoelastic Models of Porcine Skin and Its Gelatin-Based Surrogates. *Mechanics of Materials*, **177**, Article ID: 104559. https://doi.org/10.1016/j.mechmat.2023.104559

[7] Lavigne, T., Urcun, S., Jacquet, E., Chambert, J., Elouneg, A., Suarez-Afanador, C.A. *et al*. (2024) Poromechanical Modelling of the Time-Dependent Response of *in Vivo* Human Skin during Extension. https://doi.org/10.48550/arXiv.2412.07374

[8] Jaiswal, S., Sigaeva, T., Nadimpalli, S.P.V., Lieber, S. and Chester, S.A. (2023) Characterization and Modeling of the Anisotropic Behavior of the Porcine Dermis. *Mechanics Research Communications*, **129**, Article ID: 104098. https://doi.org/10.1016/j.mechrescom.2023.104098

[9] Alliliche, W., Renaud, C., Cros, J. and Feng, Z. (2022) An Anisotropic Hyperelastic Model for Human Skin: Finite Element Modeling, Identification of Parameters, Mechanical Tests. In: Tavares, J.M.R.S., Bourauel, C., Geris, L. and Vander Slote, J., Eds., *Computer Methods, Imaging and Visualization in Biomechanics and Biomedical Engineering II*, Springer International Publishing, 271-280. https://doi.org/10.1007/978-3-031-10015-4_23

[10] Wiśniewska, A. and Liber-Kneć, A. (2016) Influence of a Skin Tissue Anisotropy on Mechanical Hysteresis. *Technical Transactions*, **2016**, 125-136.

[11] Langer, K. and von Edenberg, R. (1861) Zur Anatomie und Physiologie der Haut. I. Über die Spaltbarkeit der Cutis. 19-46.

[12] Alexander, H. and Cook, T.H. (1977) Accounting for Natural Tension in the Mechanical Testing of Human Skin. *Journal of Investigative Dermatology*, **69**, 310-314. https://doi.org/10.1111/1523-1747.ep12507731

[13] Pauchot, J., Servagi, S., Laveaux, C., Lasserre, G. and Tropet, Y. (2010) Couverture d'une perte de substance dorsale médiane par deux lambeaux musculocutanés de rotation de latissimus dorsi avec palette cutanée en V-Y. Bases géométriques et intérêt. À propos d'un cas. *Annales de Chirurgie Plastique Esthétique*, **55**, 66-70. https://doi.org/10.1016/j.anplas.2008.12.003

[14] Remache, D., Chambert, J., Pauchot, J. and Jacquet, E. (2015) Numerical Analysis of the V-Y Shaped Advancement Flap. *Medical Engineering & Physics*, **37**, 987-994. https://doi.org/10.1016/j.medengphy.2015.08.005

[15] Ji, X.L., Zhang, H.H. and Han, S.Y. (2023) A Merging Constitutive Relation for Skins under Uniaxial Tension. *MRS Communications*, **13**, 520-525. https://doi.org/10.1557/s43579-023-00374-x

[16] Karimi, A., Rahmati, S.M. and Navidbakhsh, M. (2015) Mechanical Characterization of the Rat and Mice Skin Tissues Using Histostructural and Uniaxial Data. *Bioengineered*, **6**, 153-160. https://doi.org/10.1080/21655979.2015.1036202

[17] Manan, N.F.A., Mahmud, J. and Ismail, M.H. (2013) Quantifying the Biomechanical Properties of Bovine Skin under Uniaxial Tension. *Journal of Medical and Bioengineering*, **2**, 45-48. https://doi.org/10.12720/jomb.2.1.45-48

[18] Delalleau, A., Josse, G., Lagarde, J., Zahouani, H. and Bergheau, J. (2007) A Nonlinear Elastic Behavior to Identify the Mechanical Parameters of Human Skin *in Vivo*. *Skin Research and Technology*, **14**, 152-164. https://doi.org/10.1111/j.1600-0846.2007.00269.x

[19] Barbenel, J.C. and Evans, J.H. (1977) The Time-Dependent Mechanical Properties of Skin. *Journal of Investigative Dermatology*, **69**, 318-320. https://doi.org/10.1111/1523-1747.ep12507759

[20] Remache, D. (2013) Contribution à l'étude expérimentale et numérique du comportement hyperélastique et anisotrope de la peau humaine. https://theses.hal.science/tel-01117057

[21] Choi, J., Kim, S., Rhim, S. and Rhee, K. (2019) Determination of Uniaxial Tensile Behavior of Hypodermis in Porcine Skin Based on Rule of Mixtures. *Archives of Metallurgy and Materials*, **64**, 491-494. https://doi.org/10.24425/amm.2019.127565

[22] Agache, P.G., Monneur, C., Leveque, J.L. and De Rigal, J. (1980) Mechanical Properties and Young's Modulus of Human Skin *in Vivo*. *Archives of Dermatological Research*, **269**, 221-232. https://doi.org/10.1007/bf00406415

[23] Edwards, C. and Marks, R. (1995) Evaluation of Biomechanical Properties of Human Skin. *Clinics in Dermatology*, **13**, 375-380. https://doi.org/10.1016/0738-081x(95)00078-t

[24] Boyer, G., Pailler Mattei, C., Molimard, J., Pericoi, M., Laquieze, S. and Zahouani, H. (2012) Non Contact Method for *in Vivo* Assessment of Skin Mechanical Properties for Assessing Effect of Ageing. *Medical Engineering & Physics*, **34**, 172-178. https://doi.org/10.1016/j.medengphy.2011.07.007

[25] Lanir, Y., Dikstein, S., Hartzshtark, A. and Manny, V. (1990) *In- Vivo* Indentation of Human Skin. *Journal of Biomechanical Engineering*, **112**, 63-69. https://doi.org/10.1115/1.2891127

[26] Payne, P.A. (1991) Measurement of Properties and Function of Skin. *Clinical Physics and Physiological Measurement*, **12**, 105-129. https://doi.org/10.1088/0143-0815/12/2/001

[27] Hendriks, F.M., Brokken, D., Van Eemeren, J.T.W.M., Oomens, C.W.J., Baaijens, F.P.T. and Horsten, J.B.A.M. (2003) A Numerical-Experimental Method to Characterize the Non-Linear Mechanical Behaviour of Human Skin: Non-Linear Mechanical Behaviour of Human Skin. *Skin Research and Technology*, **9**, 274-283. https://doi.org/10.1034/j.1600-0846.2003.00019.x

[28] Diridollou, S., Patat, F., Gens, F., Vaillant, L., Black, D., Lagarde, J.M., *et al*. (2000) *In Vivo* Model of the Mechanical Properties of the Human Skin under Suction. *Skin Research and Technology*, **6**, 214-221. https://doi.org/10.1034/j.1600-0846.2000.006004214.x

[29] Agache, P.G. (2000) Physiologie de la peau et explorations fonctionnelles cutanées

[Internet]. Editions médicales internationales; Technique & documentation.

[30] Yuan, Z. and Zhong, Z. (2024) A Constitutive Model for Softening Behaviors of Skin Tissue. *Acta Mechanica Solida Sinica*, **37**, 762-770. https://doi.org/10.1007/s10338-024-00474-8

[31] Barsimantov, J., Payne, J., de Lucio, M., Hakim, M., Gomez, H., Solorio, L., *et al*. (2024) Poroelastic Characterization and Modeling of Subcutaneous Tissue under Confined Compression. *Annals of Biomedical Engineering*, **52**, 1638-1652. https://doi.org/10.1007/s10439-024-03477-1

[32] Marckmann, G. (2004) Contribution à l'étude des élastomères et des membranes soufflées. These de doctorat, Nantes.

[33] Wex, C., Arndt, S., Stoll, A., Bruns, C. and Kupriyanova, Y. (2015) Isotropic Incompressible Hyperelastic Models for Modelling the Mechanical Behaviour of Biological Tissues: A Review. *Biomedical Engineering/Biomedizinische Technik*, **60**, 577-592. https://doi.org/10.1515/bmt-2014-0146

[34] Martins, P.A.L.S., Natal Jorge, R.M. and Ferreira, A.J.M. (2006) A Comparative Study of Several Material Models for Prediction of Hyperelastic Properties: Application to Silicone-Rubber and Soft Tissues. *Strain*, **42**, 135-147. https://doi.org/10.1111/j.1475-1305.2006.00257.x

[35] Łagan, S.D. and Liber-Kneć, A. (2017) Experimental Testing and Constitutive Modeling of the Mechanical Properties of the Swine Skin Tissue. *Acta of Bioengineering and Biomechanics*, **19**, 93-102.

[36] Gunner, C.W., Hutton, W.C. and Burlin, T.E. (1979) The Mechanical Properties of Skin *in Vivo*—A Portable Hand-Held Extensometer. *British Journal of Dermatology*, **100**, 161-163. https://doi.org/10.1111/j.1365-2133.1979.tb05555.x

[37] Bischoff, J.E., Arruda, E.M. and Grosh, K. (2000) Finite Element Modeling of Human Skin Using an Isotropic, Nonlinear Elastic Constitutive Model. *Journal of Biomechanics*, **33**, 645-652. https://doi.org/10.1016/s0021-9290(00)00018-x

[38] Lim, J., Hong, J., Chen, W.W. and Weerasooriya, T. (2011) Mechanical Response of Pig Skin under Dynamic Tensile Loading. *International Journal of Impact Engineering*, **38**, 130-135. https://doi.org/10.1016/j.ijimpeng.2010.09.003

[39] Beda, T. (2006) Combining Approach in Stages with Least Squares for Fits of Data in Hyperelasticity. *Comptes Rendus. Mécanique*, **334**, 628-633. https://doi.org/10.1016/j.crme.2006.06.004

[40] Nunes, L.C.S. and Moreira, D.C. (2013) Simple Shear under Large Deformation: Experimental and Theoretical Analyses. *European Journal of Mechanics A/Solids*, **42**, 315-322. https://doi.org/10.1016/j.euromechsol.2013.07.002

[41] Bien-aimé, L.K.M., Blaise, B.B. and Beda, T. (2020) Characterization of Hyperelastic Deformation Behavior of Rubber-Like Materials. *SN Applied Sciences*, **2**, Article No. 648. https://doi.org/10.1007/s42452-020-2355-6

[42] Wu, Y., Wang, H. and Li, A. (2016) Parameter Identification Methods for Hyperelastic and Hyper-Viscoelastic Models. *Applied Sciences*, **6**, Article No. 386. https://doi.org/10.3390/app6120386

[43] Madahan Bien-Aimé, L.K., Blaise, B. and Beda, T. (2019) Comparison of Continuum Constitutive Hyperelastic Models Based on Exponential Forms. *International Journal of Innovative Science and Research Technology*, **4**, 1360-1367.

[44] Beda, T. and Chevalier, Y. (2003) Non-Linear Approximation Method by an Approach in Stages. *Computational Mechanics*, **32**, 177-184. https://doi.org/10.1007/s00466-003-0473-9

[45] Fernández, J.R., López-Campos, J.A., Segade, A. and Vilán, J.A. (2018) A Genetic Algorithm for the Characterization of Hyperelastic Materials. *Applied Mathematics and Computation*, **329**, 239-250. https://doi.org/10.1016/j.amc.2018.02.008

[46] Blaise, B.B., Betchewe, G. and Beda, T. (2019) Optimization of the Model of Ogden Energy by the Genetic Algorithm Method. *Applied Rheology*, **29**, 21-29. https://doi.org/10.1515/arh-2019-0003

[47] Dya, T., Blaise, B.B., Betchewe, G. and Alidou, M. (2021) Implementation of Particle Swarm Optimization Algorithm in Matlab Code for Hyperelastic Characterization. *World Journal of Mechanics*, **11**, 146-163. https://doi.org/10.4236/wjm.2021.117011